Available online at www.sciencedirect.com
ScienceDirect
Journal of Solid State Chemistry 180 (2007) 1372–1380
JOURNAL OF SOLID STATE CHEMISTRY
www.elsevier.com/locate/jssc

The extended chain compounds $Ln_{12}(C_2)_3I_{17}$ (Ln = Pr, Nd, Gd, Dy): Synthesis, structure and physical properties

Mikhail Ryazanov, Hansjürgen Mattausch, Arndt Simon*

Max-Planck-Institut für Festkörperforschung, Heisenbergstr. 1, D-70569 Stuttgart, Germany

Received 11 December 2006; received in revised form 24 January 2007; accepted 28 January 2007
Available online 8 February 2007

Dedicated to Professor Wolf Bronger on the occasion of his 75th birthday

Abstract

The title compounds are obtained in high yield from stoichiometric mixtures of Ln, LnI_3 and graphite, heated at 900–950 °C in welded Ta containers. The crystal structures of new Pr and Nd phases determined by single-crystal X-ray diffraction are related to those of other $Ln_{12}(C_2)_3I_{17}$-type compounds ($C\,2/c$, $a = 19.610(1)$ and $19.574(4)$ Å, $b = 12.406(2)$ and $12.393(3)$ Å, $c = 19.062(5)$ and $19.003(5)$ Å, $\beta = 90.45(3)^\circ$ and $90.41(3)^\circ$, for $Pr_{12}(C_2)_3I_{17}$ and $Nd_{12}(C_2)_3I_{17}$, respectively). All compounds contain infinite zigzag chains of C_2-centered metal atom octahedra condensed by edge-sharing into the $[tcc]_\infty$ sequence (c = *cis*, t = *trans*) and surrounded by edge-bridging iodine atoms as well as by apical iodine atoms that bridge between chains. The polycrystalline $Gd_{12}(C_2)_3I_{17}$ sample exhibits semiconducting thermal behavior which is consistent with an ionic formulation $(Ln^{3+})_{12}(C_2^{6-})_3(I^-)_{17}(e^-)$ under the assumption that one extra electron is localized in metal–metal bonding. The magnetization measurements on $Nd_{12}(C_2)_3I_{17}$, $Gd_{12}(C_2)_3I_{17}$ and $Dy_{12}(C_2)_3I_{17}$ indicate the coexistence of competing magnetic interactions leading to spin freezing at $T_f = 5$ K for the Gd phase. The Nd and Dy compounds order antiferromagnetically at $T_N = 25$ and 29 K, respectively. For $Dy_{12}(C_2)_3I_{17}$, a metamagnetic transition is observed at a critical magnetic field $H \approx 25$ kOe.

Keywords: Rare earth metal carbide halides; Chain-like compounds; Magnetism; Spin freezing

1. Introduction

The rare earth metal halides are known to form a large variety of reduced phases that contain metal–metal bonded species [1–4]. In most cases, the structures of these compounds are derived from Ln_6 octahedral units often comprising interstitial entities Z, which occur either as discrete clusters [5–10] or condensed into single or twin chains, layers, and, finally, three-dimensional frameworks [4]. With only one exception known so far [11], edge sharing of the Ln_6 units is observed as mode of condensation. So, Ln_{10} double octahedra in $Ln_{10}(Z)_2X_{18}$ and $Ln_{10}(Z)_2X_{17}$ [6], $Ln_{10}(Z)_2X_{16}$ [7], Ln_{14} triple octahedra in $Ln_{14}(Z)_3X_{20}$ [8], and Ln_{16} quadruple octahedra in $Ln_{16}Z_4X_{20}$ [9], $Ln_{16}(Z)_4X_{23}$ [10] occur as discrete clusters. Infinite chains exhibit different configurations derived from the cluster condensation via *cis*- and *trans*-positioned edges (see Scheme 1). In the ternary phases Ln_4ZX_5 (Z = C, C_2, B, B_4) [12–14], the chain configuration is characterized by a t–t–t sequence (1a). For compounds Ln_4ZX_6, both the t–t–t arrangement (Z = Si in Tb_4SiBr_6) [15] as well as t–c–t configuration (Z = B in Y_4BBr_6) [16] are found, obviously depending on the choice of Z. For $Gd_{12}(C_2)_3I_{17}$ and isotypic $Ln_{12}(C_2)_3I_{17}$ phases (Ln = La, Ce and Dy) with C_2-groups as interstitials, t–c–c chains (1c) are observed [17–20].

Compared with normal valence compounds, the metal-rich halides of the lanthanides have extra electrons, which are not localized in the 4*f* shell but rather become involved in metal–metal bonding. The combination of well localized magnetic moments on Ln atoms and itinerant electrons together with the structural diversity of the reduced halides makes these phases potential candidates to exhibit

*Corresponding author. Fax: +49 711 689 1642.
E-mail address: A.Simon@fkf.mpg.de (A. Simon).

0022-4596/$ - see front matter © 2007 Elsevier Inc. All rights reserved.
doi:10.1016/j.jssc.2007.01.029

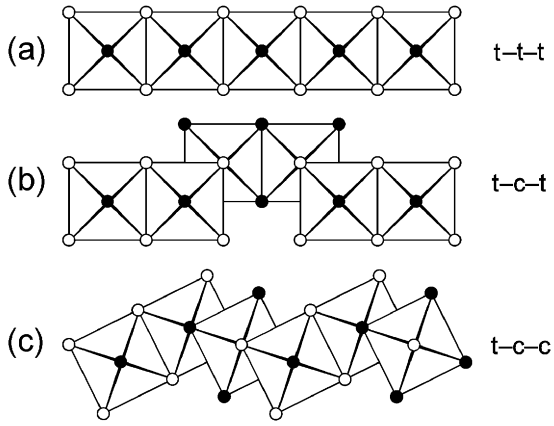

Scheme 1.

interesting physical properties associated with low-dimensional strongly correlated electron systems. In fact, the layered $M_2C_2X_2$ (M = Y, La; X = Cl, Br or I) carbide halides are superconductors with the maximum transition temperature reaching $T_c = 11.6$ K [21], while the magnetic GdH_xI_2 phases exhibit a colossal negative magnetoresistance as large as 95% at 150 K for $x \approx 0.24$ [22]. On the other hand, little is known about the physical properties of the rare earth metal-rich halides with discrete clusters or chain structures [1,13,23,24].

In this contribution, we report the syntheses and structures of two new ternary phases, $Pr_{12}(C_2)_3I_{17}$ and $Nd_{12}(C_2)_3I_{17}$, belonging to the $Ln_{12}(C_2)_3I_{17}$ family of chainlike compounds. The magnetic properties of the Nd, Gd and Dy phases are discussed. Also, the electrical properties of $Gd_{12}(C_2)_3I_{17}$ have been studied.

2. Experimental section

2.1. Preparation

Ln metal pieces (sublimed, 99.99%; Johnson Matthey, Germany), LnI_3 and graphite powder (99.95%, Aldrich) were used as starting materials. The metal ingots were mechanically cut into small pieces before being used. LnI_3 was prepared from the elements by slowly heating the reagents in evacuated sealed silica tubes and further purified by two subsequent sublimations in Ta tubes under high vacuum ($\sim 10^{-4}$ Torr). All handling was carried out under Ar atmosphere in a glovebox (M. Braun) or by employing standard Schlenk techniques.

The stoichiometric mixtures of the starting materials (LnI_3:*Ln*:C = 17:19:18) were arc-sealed in Ta tubes under Ar atmosphere. To avoid oxidation of the reaction containers, the Ta tubes were further sealed in evacuated silica jackets and then heated at temperatures between 900 and 950 °C for 1–6 weeks. All the compounds obtained are sensitive to moisture and air.

2.2. X-ray analysis

The reaction products were ground to fine powders under Ar atmosphere and sealed in glass capillaries for phase identification either by a modified Guinier technique [25] ($CuK\alpha_1$: $\lambda = 1.54056$ Å; internal standard Si with $a = 5.43035$ Å; Fujifilm BAS-5000 imaging plate system) or by using a powder diffractometer (Stoe STADI P: $CuK\alpha_1$ radiation, Ge monochromator). According to the X-ray powder diffraction analysis, all samples are single phases.

Single crystals of $Pr_{12}(C_2)_3I_{17}$ and $Nd_{12}(C_2)_3I_{17}$ were selected under Na-dried paraffin oil and sealed in glass capillaries under Ar atmosphere. They were first checked for their quality by Laue diffraction patterns before diffraction data of suitable specimens were collected on a single-crystal Stoe IPDS (Image Plate Diffraction System) instrument with graphite monochromatized $MoK\alpha$ radiation.

The structures were solved with direct methods using the program SHELXS-97 [26], and subsequently refined (full-matrix least squares on F^2) with the program SHELXL-97 [26]. All atom positions were refined anisotropically in the final refinements. Crystallographic details, atomic parameters and selected interatomic distances for $Pr_{12}(C_2)_3I_{17}$ and $Nd_{12}(C_2)_3I_{17}$ are summarized in Tables 1–5.

Further details of the crystal structure investigations can be obtained from the Fachinformationszentrum Karlsruhe, D-76334 Eggenstein-Leopoldshofen (fax: +49 7247 808 666; e-mail: crystaldata@fiz.karlsruhe.de) on quoting the depository numbers CSD-417388 for $Pr_{12}(C_2)_3I_{17}$ and CSD-417389 for $Nd_{12}(C_2)_3I_{17}$.

2.3. Electrical measurements

Electrical resistance R was determined on a pressed powder pellet of $Gd_{12}C_6I_{17}$ (diameter 5 mm, thickness $h \sim 0.5$ mm) by the van der Pauw method [28] in a temperature range of 10–290 K. The sample was pressed onto four gold-plated spring contacts within a vacuum tight cell. To evaluate approximately the resistivity values, we used the van der Pauw formula $\rho\ (\Omega\,\mathrm{cm}) \approx R\ (\Omega) h\ (\mathrm{cm}) \pi / \ln 2$.

2.4. Magnetic measurements

Measurements of the dc magnetization M were performed with a SQUID magnetometer (MPMS XL, Quantum Design) between 2 and 350 K and magnetic fields H up to 70 kOe. The polycrystalline samples were pressed to pellets (diameter 3 mm) and placed into dried gelatine capsules filled with He exchange gas to provide sufficient thermal contact. In the studies of zero-field-cooled (zfc) susceptibilities ($\chi_{dc} = M/H$), the samples were first cooled from 298 to 2 K in zero field. At 2 K the external magnetic field ($100 \leqslant H \leqslant 5 \times 10^4$ Oe) was applied and then M_{zfc} was measured upon warming. The ac

Table 1
Crystal data and structure refinement for $Pr_{12}(C_2)_3I_{17}$ and $Nd_{12}(C_2)_3I_{17}$

Empirical formula	$Pr_{12}(C_2)_3I_{17}$	$Nd_{12}(C_2)_3I_{17}$
Formula weight (g/mol)	3920.28	3960.24
Crystal size (mm^3); color	$0.14 \times 0.12 \times 0.12$; silver	$0.30 \times 0.12 \times 0.12$; shiny black
Crystal system	Monoclinic	Monoclinic
Space group	$C\ 2/c$	C $2/c$
Unit cell dimensions (Å, deg)	$a = 19.610(1)$	$a = 19.574(4)$
	$b = 12.406(2)$	b = 12.393(3)
	$c = 19.062(5)$	c = 19.003(5)
	$\beta = 90.45(3)$	$\beta = 90.41(3)$
Volume ($Å^3$); Z	4637.3(14); 4	4609.6(16); 4
Calculated density (g/cm^3)	5.615	5.706
Radiation (Å)	λ (MoKα) = 0.71073	λ (MoKα) = 0.71073
Temperature (K)	293(2)	293(2)
Absorption coefficient (mm^{-1})	23.659	24.634
$F(0\,0\,0)$	6580	6628
2ϑ-range (deg)	$3.88 \leqslant 2\vartheta \leqslant 50.00$	$4.44 \leqslant 2\vartheta \leqslant 58.00$
Index range	$-23 \leqslant h \leqslant 23$	$-26 \leqslant h \leqslant 26$
	$-14 \leqslant k \leqslant 14$	$-16 \leqslant k \leqslant 16$
	$-20 \leqslant l \leqslant 22$	$-25 \leqslant l \leqslant 25$
Reflections measured/independent	29,305/4085	35,867/6127
Absorption correction	Numerical, program X-SHAPE [27]	
Transmission range	0.0514–0.2351	0.0677–0.1984
Data/parameters	4085/161	6127/161
Goodness-of-fit on F^2	1.199	1.118
Final R indices [$I \geqslant 2\sigma(I)$]	$R_1 = 0.0321$, $wR_2 = 0.0647$	$R_1 = 0.0319$, $wR_2 = 0.0563$
R indices (all data)	$R_1 = 0.0356$, $wR_2 = 0.0660$	$R_1 = 0.0429$, $wR_2 = 0.0589$
Max/min residual electron density ($e/Å^{-3}$)	1.226/−1.401	1.708/−1.660

Table 2
Atomic coordinates and equivalent isotopic displacement parameters ($Å^2$) for $Pr_{12}(C_2)_3I_{17}$

Atom	x/a	y/b	z/c	U_{eq}
Pr1	0.0751(1)	0.7354(1)	0.2111(1)	0.0152(1)
Pr2	0.0474(1)	0.9757(1)	0.3468(1)	0.0155(1)
Pr3	0.1445(1)	0.4993(1)	0.5498(1)	0.0168(1)
Pr4	0.1657(1)	0.7387(1)	0.3827(1)	0.0171(1)
Pr5	0.0423(1)	0.4918(1)	0.3708(1)	0.0146(1)
Pr6	0.0039(1)	0.7107(1)	0.4786(1)	0.0155(1)
I1	0.1035(1)	0.4727(1)	0.2087(1)	0.0205(1)
I2	0.2041(1)	0.4890(1)	0.3977(1)	0.0214(1)
I3	0.1074(1)	0.9942(1)	0.1955(1)	0.0213(1)
I4	0.2385(1)	0.7353(1)	0.2437(1)	0.0277(1)
I5	0.1546(1)	0.2431(1)	0.0512(1)	0.0223(1)
I6	0.1500(1)	0.7534(1)	0.0574(1)	0.0217(1)
I7	0	0	0.5	0.0375(1)
I8	0.0458(1)	0.2372(1)	0.3592(1)	0.0327(2)
I9	0.1970(1)	0.9905(1)	0.3993(1)	0.0314(2)
C1	0.0339(4)	0.5014(6)	0.5116(4)	0.0142(16)
C2	0.0449(4)	0.7907(6)	0.3474(4)	0.0126(15)
C3	0.0440(4)	0.6780(6)	0.3504(4)	0.0152(16)

U_{eq} is defined as one-third of the trace of the orthogonalized U_{ij} tensor.

Table 3
Atomic coordinates and equivalent isotopic displacement parameters ($Å^2$) for $Nd_{12}(C_2)_3I_{17}$

Atom	x/a	y/b	z/c	U_{eq}
Nd1	0.0748(1)	0.7352(1)	0.2113(1)	0.0136(1)
Nd2	0.0475(1)	0.9750(1)	0.3468(1)	0.0137(1)
Nd3	0.1442(1)	0.4997(1)	0.5499(1)	0.0150(1)
Nd4	0.1648(1)	0.7385(1)	0.3826(1)	0.0154(1)
Nd5	0.0421(1)	0.4915(1)	0.3713(1)	0.0130(1)
Nd6	0.0035(1)	0.7098(1)	0.4785(1)	0.0138(1)
I1	0.1033(1)	0.4723(1)	0.2086(1)	0.0187(1)
I2	0.2039(1)	0.4891(1)	0.3979(1)	0.0194(1)
I3	0.1069(1)	0.9944(1)	0.1955(1)	0.0194(1)
I4	0.2384(1)	0.7350(1)	0.2441(1)	0.0258(1)
I5	0.1540(1)	0.2433(1)	0.0508(1)	0.0204(1)
I6	0.1501(1)	0.7525(1)	0.0576(1)	0.0198(1)
I7	0	0	0.5	0.0355(2)
I8	0.0463(1)	0.2374(1)	0.3595(1)	0.0296(1)
I9	0.1970(1)	0.9897(1)	0.3991(1)	0.0286(1)
C1	0.0344(3)	0.5005(5)	0.5123(3)	0.0120(11)
C2	0.0452(3)	0.7919(5)	0.3477(3)	0.0118(11)
C3	0.0445(3)	0.6762(5)	0.3502(3)	0.0138(11)

U_{eq} is defined as one third of the trace of the orthogonalized U_{ij} tensor.

magnetic susceptibility data (1 Oe ac magnetic field, $\omega = 100$ Hz) were collected on the same instrument in the temperature range $2 \leqslant T \leqslant 350$ K. The frequency dependence of χ_{ac} was studied at temperatures from 2 to 10 K upon varying the measurement frequency ω between 10, 100 and 1000 Hz.

3. Results and discussion

3.1. Crystal structure

The ternary compounds $Ln_{12}(C_2)_3I_{17}$ (Ln = La [18], Ce [19], Pr, Nd, Gd [17] and Dy [20]) constitute a family of

Table 4
Selected interatomic distances (Å) for $Pr_{12}(C_2)_3I_{17}$

$Pr_{12}(C_2)_3I_{17}$					
Pr1	Pr1	3.308(1)	Pr3	I9	3.251(1)
	Pr2	3.979(1)		C1	2.283(7)
	Pr2	3.987(1)	Pr4	Pr5	3.909(1)
	Pr4	3.710(1)		Pr6	3.690(1)
	Pr5	4.100(1)		I2	3.200(1)
	Pr5	4.342(1)		I4	3.019(1)
	Pr6	3.934(1)		I5	3.230(1)
	I1	3.307(1)		I5	3.733(1)
	I3	3.286(1)		I9	3.200(1)
	I4	2.260(1)		C2	2.540(7)
	I6	2.295(1)		C3	2.573(7)
	C2	2.684(7)	Pr5	Pr6	3.491(1)
	C2	2.756(7)		Pr6	3.926(1)
	C3	2.699(7)		I1	3.234(1)
	C3	2.821(8)		I1	3.332(1)
Pr2	Pr4	3.804(1)		I2	3.210(1)
	Pr6	4.229(1)		I8	3.166(1)
	I3	3.131(1)		C1	2.692(8)
	I3	3.143(1)		C1	2.705(8)
	I7	3.087(1)		C3	2.344(8)
	I8	3.253(1)	Pr6	I5	3.304(1)
	I9	3.098(1)		I6	3.135(1)
	C2	2.297(8)		I7	3.613(1)
Pr3	Pr5	3.945(1)		I8	3.313(1)
	Pr5	3.975(1)		C1	2.735(8)
	Pr6	3.941(1)		C1	2.741(8)
	Pr6	4.033(1)		C2	2.814(7)
	I1	3.158(1)		C3	2.604(8)
	I2	3.139(1)	C1	C1	1.398(15)
	I5	3.203(1)	C2	C3	1.399(11)
	I6	3.139(1)			

Table 5
Selected interatomic distances (Å) for $Nd_{12}(C_2)_3I_{17}$

$Nd_{12}(C_2)_3I_{17}$					
Nd1	Nd1	3.287(1)	Nd3	I9	3.252(1)
	Nd2	3.969(1)		C1	2.260(5)
	Nd2	3.971(1)	Nd4	Nd5	3.896(1)
	Nd4	3.689(1)		Nd6	3.674(1)
	Nd5	4.094(1)		I2	3.197(1)
	Nd5	4.336(1)		I4	3.009(1)
	Nd6	3.922(1)		I5	3.214(1)
	I1	3.306(1)		I5	3.758(1)
	I3	3.288(1)		I9	3.191(1)
	I4	2.257(1)		C2	2.516(6)
	I6	2.287(1)		C3	2.548(7)
	C2	2.689(6)	Nd5	Nd6	3.472(1)
	C2	2.752(6)		Nd6	3.898(1)
	C3	2.705(6)		I1	3.225(1)
	C3	2.808(6)		I1	3.333(1)
Nd2	Nd4	3.781(1)		I2	3.204(1)
	Nd6	4.225(1)		I8	3.159(1)
	I3	3.118(1)		C1	2.682(8)
	I3	3.132(1)		C1	2.686(8)
	I7	3.079(1)		C3	2.324(8)
	I8	3.260(1)	Nd6	I5	3.294(1)
	I9	3.088(1)		I6	3.124(1)
	C2	2.271(6)		I7	3.621(1)
Nd3	Nd5	3.928(1)		I8	3.301(1)
	Nd5	3.953(1)		C1	2.716(6)
	Nd6	3.920(1)		C1	2.738(6)
	Nd6	4.019(1)		C2	2.812(6)
	I1	3.145(1)		C3	2.605(6)
	I2	3.125(1)	C1	C1	1.423(11)
	I5	3.191(1)	C2	C3	1.434(8)
	I6	3.131(1)			

interstitially stabilized lanthanide halides whose structures are characterized by zigzag chains of condensed Ln_6Z octahedra with interstitial C_2 units. Infinite chains are formed from edge-sharing Ln_6 octahedra shown in Fig. 1 for $Pr_{12}(C_2)_3I_{17}$, which are capped by I atoms above all free edges as in the M_6X_{12}-type cluster. The condensation of octahedra in a t–c–c sequence leads to folded $^1_\infty[Pr_{10}(C_2)_2Pr_2(C_2)]$ chains. Such chains run parallel to the *c*-axis and are interconnected via bridging I^{i-i} and I^{i-a} atoms [29]. The shortest interchain metal–metal distances are 5.22 and 5.23 Å for the Pr and Nd compounds, respectively. The *Ln*–*Ln* distances in the chain vary from 3.31 to 4.34 Å in $Pr_{12}(C_2)_3I_{17}$, and from 3.28 to 4.34 Å in $Nd_{12}(C_2)_3I_{17}$. Similar as in other $Ln_{12}(C_2)_3I_{17}$ compounds, the shortest *Ln*–*Ln* distances are between the metal atoms forming the common edges, while the other *Ln*–*Ln* distances are at least 0.3 Å longer (cf. Tables 4 and 5). The interstitial C_2 dumbbells are directed toward those corners of the Ln_6 octahedra which are not involved in the cluster condensations. The C–C bond distances, $d_{C-C} = 1.40(1)$ Å for the Pr derivative and $1.42\,Å \leqslant d_{C-C} \leqslant 1.44$ Å for the Nd derivative, are comparable with those in other $Ln_{12}(C_2)_3I_{17}$ compounds (see Table 6). These values correspond to shortened C–C single bonds, thus suggesting the ionic formulation $(Ln^{3+})_{12}(C_2^{6-})_3(I^-)_{17}(e^-)$ with some backbonding from the occupied $C_2\pi^*$ states into *Ln* d states and one extra electron being involved in metal–metal bonding.

Finally, the systematic decrease in the cell volumes and in the mean values of the *Ln*–*Ln*, *Ln*–I and *Ln*–C bond lengths within the $Ln_{12}(C_2)_3I_{17}$ family for increasing atomic number of *Ln* is in full accordance with the expected lanthanide contraction (Table 6).

3.2. Physical properties

To study the electrical properties, we have chosen $Gd_{12}C_6I_{17}$ as a representative example of the $Ln_{12}C_6I_{17}$ family of compounds. The powder sample of $Gd_{12}C_6I_{17}$ exhibits semiconducting behavior with the electrical resistivity increasing from a room temperature value of $\sim 3 \times 10^4\,\Omega$ cm to values of $\sim 10^8\,\Omega$ cm at 120 K (Fig. 2). A least-squares fit of the data with an Arrhenius law, $\rho = \rho_o \exp(E_a/k_BT)$, yields an activation energy of 0.2 eV. The observed semiconducting behavior is consistent with the formal charge distribution $(Gd^{3+})_{12}(C_2^{6-})_3(I^-)_{17}(e^-)$, given that one extra electron per formula unit is localized in the bonds along the shared edges between the $[Gd_6(C_2)]$ units. This conclusion is also in accordance with the finding

that the Gd–Gd distances of the shared edges are considerably shorter than the remaining ones.

The magnetic behavior of $Gd_{12}(C_2)_3I_{17}$ has been characterized by magnetization measurements on polycrystalline samples in applied dc and ac magnetic fields.

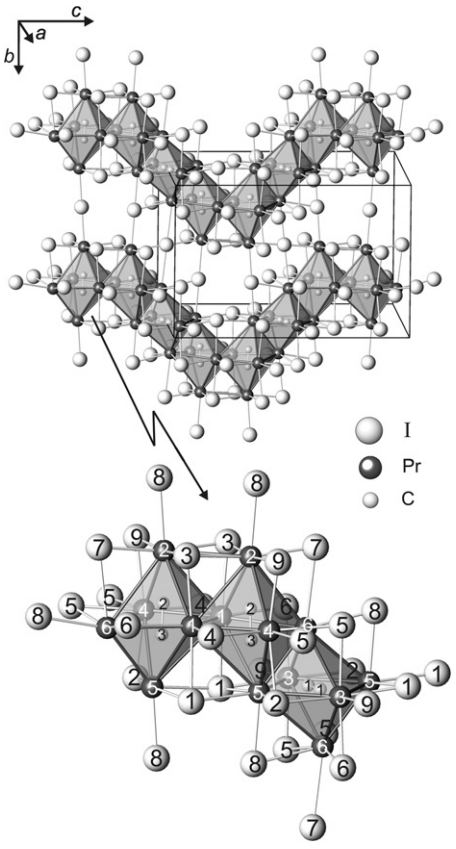

Fig. 1. Fragment of the infinite zigzag chains of edge-sharing metal atom octahedra in $Pr_{12}(C_2)_3I_{17}$. The unit cell and atom labeling scheme are shown.

Fig. 3 displays the temperature dependence of the dc magnetic susceptibility, χ_m, which increases gently as the temperature decreases to 30 K, and passes through an inflection point at around 25 K before reaching a value of ~0.25 emu/mol at 2 K. Furthermore, there is a small thermal hysteresis between zfc and field-cooled (fc) susceptibilities below 6 K. The high-temperature data follow a Curie–Weiss law, $\chi_m = C/(T-\theta)$, between 250 and 350 K giving $C = 8.29(1)\,cm^3\,K/mol$ (per Gd^{3+} ion) and $\theta = 34(1)$ (see Fig. 4). The Curie constant, C, agrees fairly well with the theoretical value ($7.88\,cm^3\,K/mol$) for magnetically isolated $S = 7/2$ ions. The positive Curie–Weiss parameter, θ, indicates that ferromagnetic (fm) interactions are prevalent at high temperatures. On the other hand, as shown in Fig. 4, the curve $\chi_m T$ vs. T quickly decreases below 100 K, thus reflecting that the antiferromagnetic (afm) exchange becomes dominant at low temperatures. This conclusion is also supported by the magnetization data collected at 1.8 K as a function of increasing magnetic field (Fig. 5). The magnetization per Gd atom increases progressively with H to reach a value of $2.3\,\mu_B$/Gd at 70 kOe, which is much smaller than the expected one for a parallel alignment of the Gd magnetic moments ($M_s = 7\,\mu_B$).

The relatively strong fm interactions between the Gd moments are likely due to indirect exchange via the d electrons involved in the localized metal–metal bonding, while the afm coupling is mediated by superexchange via $(C_2)^{6-}/I^-$ anions. The nature of the d electron mediated magnetic exchange between the $4f^7$ moments depends on whether unpaired bonding electrons or closed shells of valence electrons are involved in the exchange interaction. The first case favors fm coupling, whereas afm exchange is expected for the second case [30]. As one can infer from the metal–metal distance distribution observed in $Ln_{12}(C_2)_3I_{17}$, the extra electron would mainly occupy the metal–metal

Table 6
Characteristic structural data for $Ln_{12}(C_2)_3I_{17}$

Compound (Ref.)	Lattice parameters (Å, deg)		V (Å^3)	d_{Ln-Ln}[a] (Å)	d_{Ln-I} (Å)	d_{Ln-C} (Å)	d_{C-C} (Å)
$La_{12}(C_2)_3I_{17}$ [17]	$a = 19.927(1)$, $c = 19.399(1)$,	$b = 12.636(1)$ $\beta = 90.24(1)$	4884.58	3.403(1)–4.424(1)	3.078(1)–3.658(1)	2.347(4)–2.873(4)	1.387(7)–1.394(6)
$Ce_{12}(C_2)_3I_{17}$ [18]	$a = 19.731(4)$, $c = 19.182(4)$,	$b = 12.495(3)$ $\beta = 90.36(3)$	4729.01	3.337(1)–4.368(1)	3.042(1)–3.627(1)	2.313(4)–2.830(4)	1.386(6)–1.403(5)
$Pr_{12}(C_2)_3I_{17}$	$a = 19.610(1)$, $c = 19.062(5)$,	$b = 12.406(2)$ $\beta = 90.45(3)$	4637.29	3.307(1)–4.342(1)	3.019(1)–3.613(1)	2.283(7)–2.814(7)	1.40(1)
$Nd_{12}(C_2)_3I_{17}$	$a = 19.574(4)$, $c = 19.003(5)$,	$b = 12.393(3)$ $\beta = 90.41(3)$	4609.64	3.286(1)–4.336(1)	3.009(1)–3.621(1)	2.260(5)–2.812(6)	1.42(1)–1.434(8)
$Gd_{12}(C_2)_3I_{17}$ [16]	$a = 19.297(9)$, $c = 18.635(5)$,	$b = 12.201(5)$ $\beta = 90.37(3)$	4387.38	3.187(1)–4.269(1)	2.943(1)–3.627(1)	2.21(4)–2.72(4)	1.41(1)–1.45(1)
$Dy_{12}(C_2)_3I_{17}$ [19]	$a = 19.149(4)$, $c = 18.595(4)$,	$b = 12.069(2)$ $\beta = 90.54(3)$	4297.29	3.146(1)–4.243(1)	2.930(1)–3.558(1)	2.18(1)–2.75(1)	1.43(2)–1.435(2)

[a]Shortest distances within the Ln_6-octahedra.

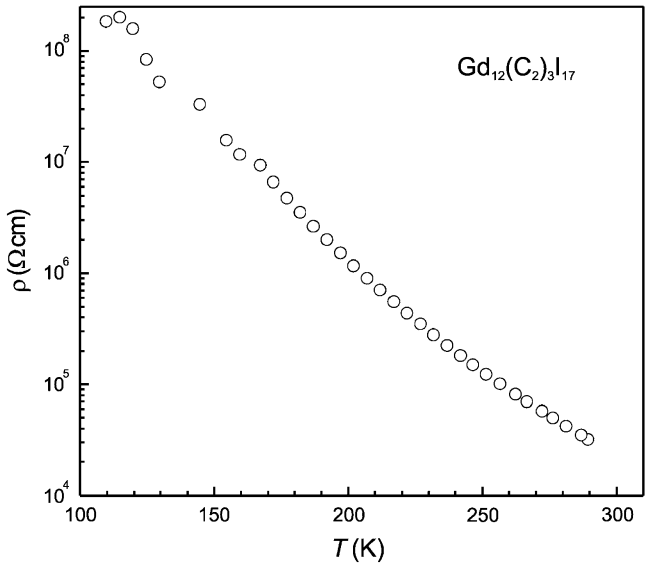

Fig. 2. Temperature dependence of the electrical resistivity of $Gd_{12}(C_2)_3I_{17}$.

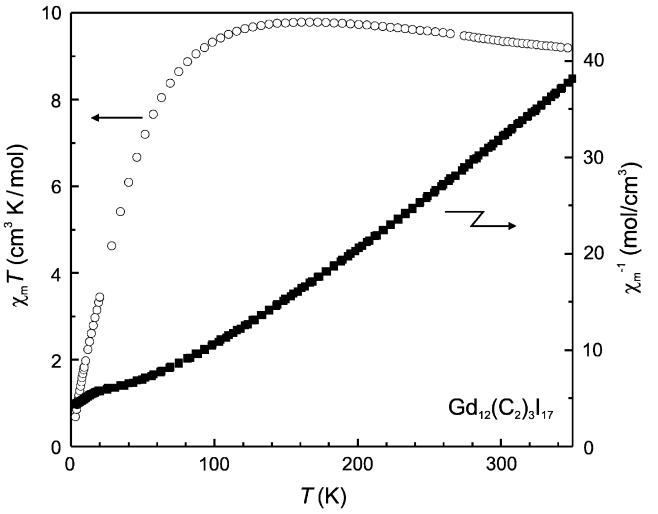

Fig. 4. Temperature dependencies of the $\chi_m T$ product and inverse susceptibility for $Gd_{12}(C_2)_3I_{17}$ at $H = 10$ kOe.

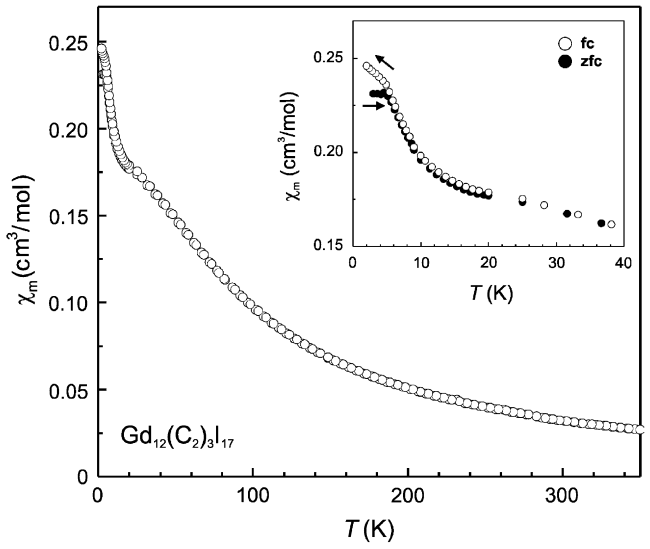

Fig. 3. Magnetic susceptibility (M/H) vs. temperature for $Gd_{12}(C_2)_3I_{17}$ in an applied field of 100 Oe. The inset shows the difference between zero-field-cooled (zfc) and field-cooled (fc) susceptibilities at low temperatures.

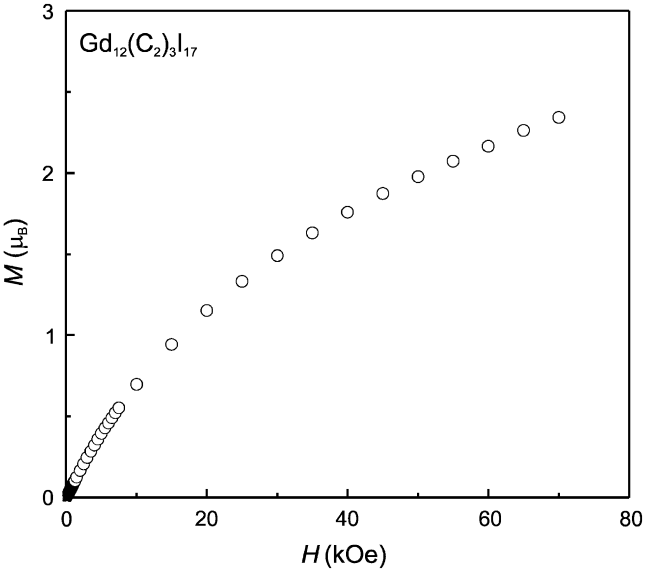

Fig. 5. Magnetization (per Gd atom) vs. field for $Gd_{12}(C_2)_3I_{17}$ at 1.8 K.

bond concentrated along the shared edges of the bioctahedral $Gd_{10}(C_2)_2I_{17}$ structural blocks. A similar conclusion has been drawn from electronic structure calculations on discrete $Gd_{10}(C_2)_2Cl_{17}$ clusters and the $Gd_{12}(C_2)_3I_{17}$ phase [31]. Here, it is worth noting that another metal-rich chain like compound of composition Gd_2Cl_3, in which all metal–metal bonding orbitals are fully occupied [32], exhibits afm behavior with a large negative θ [1,23].

The presence of competing magnetic interactions is known to induce spin frustration, leading to spin-relaxation behavior. In order to gain a better understanding of the nature of the low-temperature magnetic state, we have performed ac magnetic measurements (Fig. 6). With decreasing temperature, a maximum appears in the real part of the ac susceptibility (χ') at 5 K, the latter being defined as the magnetic freezing temperature. This anomaly is accompanied by a dissipative signal (χ'') that becomes non-zero at temperatures below 6 K and passes through a broad maximum at around 4 K. Both the χ' and χ'' peaks are frequency dependent. They shift towards higher temperatures with increasing frequency, ω. The relative frequency shift of T_f (~0.02 per decade ω) is too small to be attributed to superparamagnetic behavior and is comparable to the values commonly found in insulating spin glasses and cluster glass systems [33]. The observed "glassy" behavior in $Gd_{12}C_6I_{17}$ is associated with spin freezing at $T_f = 5$ K, caused by competing fm and afm interactions.

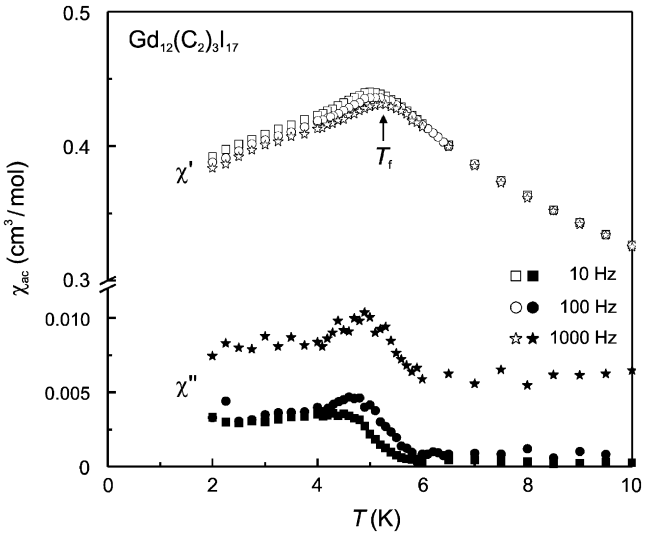

Fig. 6. Temperature dependencies of the real and imaginary components of the ac magnetic susceptibility of $Gd_{12}(C_2)_3I_{17}$ in a 1 Oe ac magnetic field at various frequencies. The freezing temperature T_f is defined as the maximum in $\chi'(T)$.

The magnetic properties of the Nd and Dy compounds are presented in Figs. 7 and 8. The high-temperature susceptibilities ($200 \leqslant T \leqslant 330$ K) follow the Curie–Weiss law with positive values of θ. The calculated values of the effective magnetic moments are in good agreement with the theoretical ones of the tripositive lanthanide ions (see Table 7). At low temperatures, both compounds exhibit a common feature, that is a maximum in the temperature dependence of the dc magnetic susceptibility appearing at 25 K (for $Nd_{12}(C_2)_3I_{17}$) and ca. 29 K (for $Dy_{12}(C_2)_3I_{17}$) as the samples are cooled in the applied field (fc mode). Zero-field-cooled measurements indicate a slight irreversibility between the fc and zfc susceptibilities at low temperatures for $Nd_{12}(C_2)_3I_{17}$, which is much more pronounced for $Dy_{12}(C_2)_3I_{17}$. The divergence between fc and zfc curves is most likely due to crystal-field anisotropies which become relevant for magnetic ions with a non-zero orbit angular moment. We attribute the observed peaks in $\chi(T)$ to the onset of long-range afm ordering, based on the following findings. With increasing applied field strength, the susceptibility anomalies shift downwards in temperature, as is expected for an antiferromagnet. The low-temperature magnetization curve of $Nd_{12}(C_2)_3I_{17}$ taken at $T = 5$ K increases almost linearly as a function of external field with a change in slope at ca. 50 kOe, reaching a maximal value of 0.4 μ_B/Nd at 70 kOe (Fig. 7b). The $Dy_{12}(C_2)_3I_{17}$ sample exhibits metamagnetic behavior with a characteristic step-like transition in the M vs H curve, as shown in Fig. 8b. The transition from afm to fm ordering occurs at a critical field of 25 kOe. The saturation magnetic moment at $H = 70$ kOe is 3.8 μ_B/Dy, i.e., 2.6 times smaller than the expected value $M_s = g \times J = 10\,\mu_B$/Dy, thus implying a noncollinear spin arrangement or a magnetic moment reduction due to crystal-field effects and pronounced structural anisotropy. The magnetic ground state in

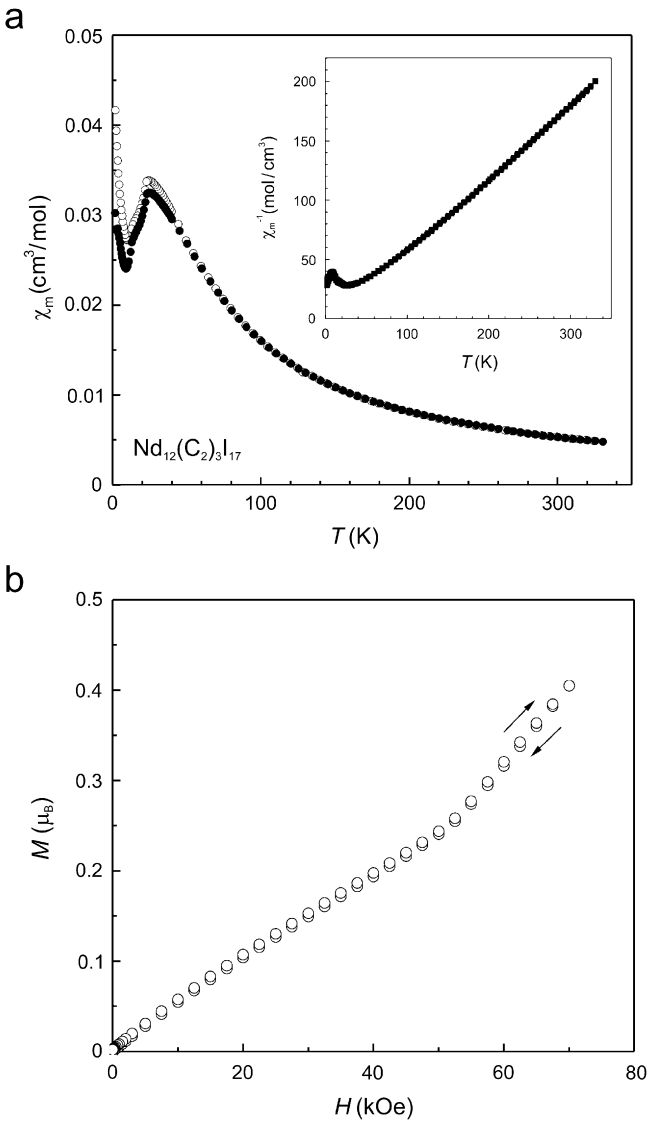

Fig. 7. (a) Magnetic susceptibility (per mol of Nd) vs. T for $Nd_{12}(C_2)_3I_{17}$ measured under $H = 100$ Oe in field-cooled (open circles) and zero-field-cooled (filled circles) mode. The inset shows the inverse magnetic susceptibility as a function of temperature. (b) Magnetization (per Nd atom) vs field for $Nd_{12}(C_2)_3I_{17}$ at 5 K.

$Ln_{12}(C_2)_3I_{17}$ (Ln = Nd, Dy) cannot be purely afm because of the positive θ values derived from the Curie–Weiss fits. This suggests that fm correlations persist in the ordered afm state, probably leading to a complicated magnetic structure.

In summary, two new members of the homologous series of compounds $Ln_{12}(C_2)_3I_{17}$ have been structurally characterized. Magnetic studies of the Gd, Nd, and Dy phases indicate mixed fm and afm interactions in the title compounds. Even though fm exchange is dominant and leads to positive θ values, the Dy and Ny compounds with large magnetocrystalline anisotropy undergo a long-range afm ordering at low temperatures, while $Gd_{12}(C_2)_3I_{17}$ exhibits spin-freezing characteristics below the transition temperature $T_f = 5$ K.

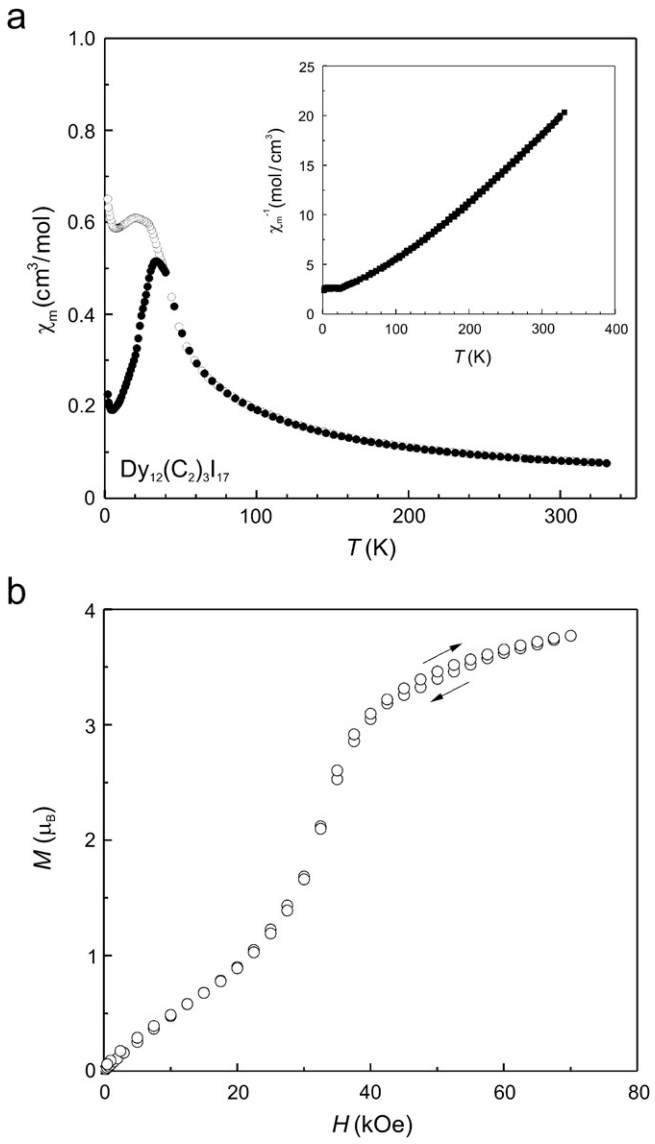

Fig. 8. (a) Magnetic susceptibility (per mol of Dy) vs. T for $Dy_{12}(C_2)_3I_{17}$ measured under $H = 100$ Oe in field-cooled (open circles) and zero-field-cooled (filled circles) mode. The inset shows the inverse magnetic susceptibility at $H = 50$ kOe as a function of temperature. (b) Magnetization (per Dy atom) vs. field for $Dy_{12}(C_2)_3I_{17}$ at 5 K.

Table 7
Characteristic magnetic parameters for $Ln_{12}(C_2)_3I_{17}$ (Ln = Nd, Gd and Dy)

Compound	T_{order} (K)	θ (K)	μ_{eff} (μ_B)	μ_{calc}[a] (μ_B)	M_s (5 K)[b] (μ_B)
$Nd_{12}(C_2)_3I_{17}$	25 (T_N)	18	3.5	3.62	0.4
$Gd_{12}(C_2)_3I_{17}$	5 (T_f)	34	8.1	7.94	2.3
$Dy_{12}(C_2)_3I_{17}$[c]	29 (T_N)	42	10.7	10.64	3.8

[a]The theoretical magnetic moments according to $\mu_{calc} = g_J\sqrt{J(J+1)}\mu_B$.
[b]Magnetization moments at $H = 70$ kOe.
[c]The $\chi(T)$ data above 150 K were found to be field dependent. This effect is most likely to originate from a small contamination of ferromagnetic DyC_x carbides with T_C varying between 220 and 180 K for $0.33 \leqslant x \leqslant 0.53$ [34]. To eliminate the ferromagnetic contribution, the high-field ($H = 50$ kOe) susceptibility data were used for the Curie–Weiss analysis.

Acknowledgments

We would like to thank R. Eger for the sample preparation, E. Brücher for the magnetization measurements, and G. Siegle for measurements of the electrical resistivity.

References

[1] A. Simon, H. Mattausch, G.J. Miller, W. Bauhofer, R.K. Kremer, in: K.A. Gscheidner Jr., L. Eyring (Eds.), Handbook on the Physics and Chemistry of Rare Earths, vol. 15, Elsevier Science Publ., Amsterdam, London, New York, Tokyo, 1991, p. 191.
[2] J.D. Corbett, J. Chem. Soc., Dalton Trans. 12 (1996) 575–587.
[3] G. Meyer, Chem. Rev. 88 (1988) 93–107.
[4] A. Simon, Hj. Mattausch, M. Ryazanov, R.K. Kremer, Z. Anorg. Allg. Chem. 632 (2006) 919–929.
[5] (a) D.S. Dudis, J.D. Corbett, S.-J. Hwu, Inorg. Chem. 25 (1986) 3434–3438;
(b) T. Hughbanks, J.D. Corbett, Inorg. Chem. 27 (1988) 2022–2026.
[6] (a) E. Warkentin, R. Masse, A. Simon, Z. Anorg. Allg. Chem. 491 (1982) 323–336;
(b) M. Lulei, J.D. Martin, L.M. Hoistad, J.D. Corbett, J. Am. Chem. Soc. 119 (1997) 513–520.
[7] H. Mattausch, E. Warkentin, O. Oeckler, A. Simon, Z. Anorg. Allg. Chem. 626 (2000) 2117–2124.
[8] H. Mattausch, A. Simon, L. Kienle, C. Hoch, C. Zheng, R.K. Kremer, Z. Anorg. Allg. Chem. 632 (2006) 1661–1670.
[9] (a) M.W. Payne, M. Ebihara, J.D. Corbett, Angew. Chem. 103 (1991) 842–844;
(b) M.W. Payne, M. Ebihara, J.D. Corbett, Angew. Chem. Int. Ed. Engl. 30 (1991) 856–858.
[10] Hj. Mattausch, G.V. Vajenine, O. Oeckler, R.K. Kremer, A. Simon, Z. Anorg. Allg. Chem. 627 (2001) 2542–2546.
[11] C. Zheng, Hj. Mattausch, A. Simon, J. Alloys Compds. 338 (2002) 165–172.
[12] A. Simon, J. Solid State Chem. 57 (1985) 2–16.
[13] S.M. Kauzlarich, T. Hughbanks, J.D. Corbett, P. Klavins, R.N. Shelton, Inorg. Chem. 27 (1988) 1791–1797.
[14] Hj. Mattausch, O. Oeckler, A. Simon, Inorg. Chim. Acta 289 (1999) 174–190.
[15] Hj. Mattausch, O. Oeckler, A. Simon, Z. Kristallogr. NCS 218 (2003) 282.
[16] Hj. Mattausch, A. Simon, Z. Kristallogr. NCS 212 (1997) 99.
[17] A. Simon, E. Warkentin, Z. Anorg. Allg. Chem. 497 (1983) 79–92.
[18] Hj. Mattausch, A. Simon, Z. Kristallogr. NCS 220 (2005) 299–300.
[19] Hj. Mattausch, A. Simon, Z. Kristallogr. NCS 220 (2005) 301–302.
[20] Hj. Mattausch, C. Hoch, A. Simon, Z. Naturforsch. B 62 (2007) 148–154.
[21] (a) A. Simon, Hj. Mattausch, R. Eger, R.K. Kremer, Angew. Chem. 103 (1991) 1209–1210;
(b) A. Simon, Hj. Mattausch, R. Eger, R.K. Kremer, Angew. Chem. Int. Ed. Engl. 30 (1991) 1188–1189.
[22] (a) Felser, K. Ahn, R.K. Kremer, R. Sheshadri, A. Simon, J. Solid State Chem. 147 (1999) 19–25;
(b) M. Ryazanov, A. Simon, R.K. Kremer, H. Mattausch, Phys. Rev. B 72 (2005) 092408.
[23] R.K. Kremer, A. Simon, J. Less-Common Met. 127 (1987) 262–263.
[24] J.S. Steinwand, J.D. Corbett, J.D. Martin, Inorg. Chem. 36 (1997) 6413–6422.
[25] A. Simon, J. Appl. Crystallogr. 3 (1970) 11–18.
[26] G.M. Sheldrick, SHELXS-97 and SHELXL-97, Programs for the Solution and Refinement of Crystal Structures, University Göttingen, Germany, 1997.
[27] X-SHAPE, Crystal Optimisation for Numerical Absorption Correction, Version 1.03, Stoe & Cie GmbH, Darmstadt, Germany, 1998.

[28] L.J. van der Pauw, Philips Res. Rep. 13 (1958) 1–9.
[29] (a) H. Schäfer, H.G. Schnering, Angew. Chem. 76 (1964) 833–849;
(b) H. Schäfer, H.G. Schnering, Angew. Chem. Int. Ed. Engl. 3 (1964) 117–133.
[30] L.E. Roy, T. Hughbanks, Mater. Res. Soc. Symp. Proc. 755 (2002) 25–30.
[31] S. Satpathy, O.K. Andersen, Inorg. Chem. 24 (1985) 2604–2608.
[32] D.W. Bullett, Inorg. Chem. 24 (1985) 3319–3323.
[33] J.A. Mydosh, Spin Glasses: An Experimental Introduction, Taylor & Francis, London, 1993.
[34] Y. Aoki, D.E.G. Williams, J. Less-Common Met. 65 (1979) 35–40.